UAV Icing: The Influence of Airspeed and Chord Length on Performance Degradation

Richard Hann[1] and Tor Arne Johansen[1]

1 Centre for Autonomous Marine Operations and System (AMOS), Department of Engineering Cybernetics, Norwegian University of Science and Technology, NTNU

Abstract

Purpose –

The main objective of this manuscript is to investigate the effects of icing on UAVs at low Reynolds numbers, and to highlight the differences to icing on manned aircraft at high Reynolds numbers. This paper follows existing research on low Reynolds number effects on ice accretion. This study extends the focus to how variations of airspeed and chord length affect the ice accretions and aerodynamic performance degradation is investigated.

Design/methodology/approach – A parametric study with independent variations of airspeed and chord lengths was conducted on a typical UAV airfoil (RG-15) using icing CFD methods. FENSAP-ICE was used to simulate ice shapes and aerodynamic performance penalties. Validation was performed with two experimental ice shapes, obtained from a low-speed icing wind tunnel. Three meteorological conditions were chosen to represent the icing typologies of rime, glaze, and mixed ice. A parameter study with different chord lengths and airspeeds was then conducted for rime, glaze, and mixed icing conditions.

Findings – The simulation results showed that the effect of airspeed variation depended on the ice accretion regime. For rime, it led to a minor increase in ice accretion. For mixed and glaze the impact on ice geometry and penalties was substantially larger. The variation of chord length had a substantial impact on relative ice thicknesses, ice area, ice limits, and performance degradation, independent from the icing regime.

Research limitations/implications – The implications of this manuscript are relevant for highlighting the differences between icing on manned and unmanned aircraft. Unmanned aircraft are typically smaller and fly slower than manned aircraft. While previous research has documented the influence of this on the ice accretions, this paper investigates the effect on aerodynamic performance degradation. The findings in this work show that UAVs are more sensitive to icing conditions compared to larger and faster manned aircraft. By consequence, icing conditions are more severe for UAVs.

Practical implications – Atmospheric in-flight icing is a severe risk for fixed-wing UAVs and significantly limits their operational envelope. Since UAVs are typically smaller and operate at lower airspeeds compared to manned aircraft, it is important to understand how the differences in airspeed and size affect ice accretion and aerodynamic performance penalties.

Social implications – n/a

Originality/value – Earlier work has described the effect of Reynolds number variations on the ice accretion characteristics for UAVs. This work is expanding on those findings by investigating the effect of airspeed and chord length on ice accretion shapes separately. In addition, this study also investigates how these parameters affect aerodynamic performance penalties (lift, drag, stall).

Keywords Unmanned aerial vehicle (UAV), unmanned aerial system (UAS), icing performance penalties, ice accretion, computational fluid dynamics (CFD), low Reynolds.

Paper type: *Research paper*

1. Introduction

Unmanned aerial vehicles (UAVs) face several special challenges when it comes to atmospheric icing (Hann and Johansen, 2020). The operations of fixed-wing UAVs can be substantially limited by in-flight icing (Siquig, 1990). Such atmospheric icing can occur in many regions around the world and is a severe risk for all types of airborne vehicles (Gent, Dart and Cansdale, 2000). While the icing topic is well researched for manned aviation, few results are available for UAVs.

In general, icing leads to significant aerodynamic penalties (Bragg, Broeren and Blumenthal, 2005). Ice accretions on airfoils reduce lift, increase drag, and worsen stall behavior. This can have severe consequences on the overall aerodynamic performance of a UAV, which can even lead to the loss of the aircraft (Hann and Johansen, 2020). It is therefore important to have a good understanding of the most hazardous meteorological and flight scenarios for UAVs and how these may differ from manned aircraft.

A previous numerical study by Szilder and McIlwan (Szilder and McIlwain, 2011) studied the effect of the Reynolds number on the ice accretion process (Szilder and McIlwain, 2011). The study used a morphogenetic icing approach to simulate ice accretion over a range of Reynolds numbers from Re=5×10^4…5×10^6 on a NACA0012 airfoil in 2D. Szilder and McIlwan coupled chord length c and velocity v with a proportionality factor to investigate the Reynolds number as a single parameter in their study. They simulated ice accretion over a range of meteorological icing conditions of air temperature, LWC, and droplet sizes. Szilder and McIlwans results show that the Reynolds number has an impact on the type of ice (rime or glaze), on the total ice mass, and on the relative ice thickness. Lower Reynolds numbers lead to more rime-like ice shapes, less total ice mass, and increased relative ice thickness. Szilder and McIlwan suggested that the latter could lead to increased aerodynamic penalties, which has been shown for icing on manned aircraft at higher Reynolds numbers before (Bragg, Broeren and Blumenthal, 2005).

The objective of this paper is to extend the existing research on the effect of Reynolds number on ice accretion on UAVs to its effect on aerodynamic performance penalties. In contrast to Szilder and McIlwan, we decided to investigate the effects of airspeed and chord length independently from each other. We believe that this offered more differentiated insights into the icing mechanisms. We considered three different meteorological icing conditions for each variation of airspeed and chord length.

This study was closely related to previous work conducted at NTNU on similar topics, such as the comparison of two numerical codes for icing penalties (Hann, 2018), the effect of meteorological conditions on performance (Fajt, Hann and Lutz, 2019), experimental ice accretion results (Hann, 2019), and experimental icing performance degradation studies (Hann *et al.*, 2020). Further relevant work on icing performance degradation on UAV airfoils has been conducted by Williams et al. (Williams *et al.*, 2017) and Szilder and Yuan (Szilder and Yuan, 2017) – none of which take the effect of varying airspeeds or chord lengths into closer account.

The main objective of this work is to increase the overall understanding of which icing conditions are most hazardous for UAVs. This knowledge is an important input for example for UAV path-planning applications (Narum, Hann and Johansen, 2020) or for the design of ice protection systems (Hann *et al.*, 2019).

2. Methods

This study used the numerical icing code ANSYS FENSAP-ICE (version 2020 R1) to simulate ice accretion and aerodynamic performance penalties on lift, drag, and stall. FENSAP-ICE is a state-of-the-art computational fluid dynamic (CFD) icing tool (ANSYS, 2017). The tool has been mainly developed for icing on manned aircraft but is applied to a wide field of applications, including UAVs (Habashi *et al.*, 2004; Tran *et al.*, 2004). In this study, FENSAP-ICE was used to generate ice shapes on an airfoil and to simulate the aerodynamic icing penalties on lift and drag over a range of angles of attack. Simulations on the iced airfoils were conducted as fully-turbulent, steady-state, 2D simulations with streamline upwind artificial viscosity. Turbulence is modeled with the one-equation Spalart-Allmaras model (Spalart and Allmaras, 1992) and fully-turbulent, which is recommended for icing simulations (Chung and Addy, 2000). A variable surface roughness was calculated by FENSAP-ICE from a beading model on all iced airfoils. The clean airfoil has been simulated with free transition.The computational meshes for the icing simulation were generated with Fluent whereas the meshes for the lift and drag simulations were generated in Pointwise (version 18.2R2). Both types of meshes were a hybrid O-grid with a far-field diameter of 40·c. The boundary-layer was resolved with a regular structured grid for icing and a structured anisotropic tetrahedral extrusion (T-Rex) for the performance grid (Steinbrenner, 2015). Both meshes use a growth factor of 1.1. An example of the icing grid is given in Figure 1 and an example for the performance grid in Figure 2.

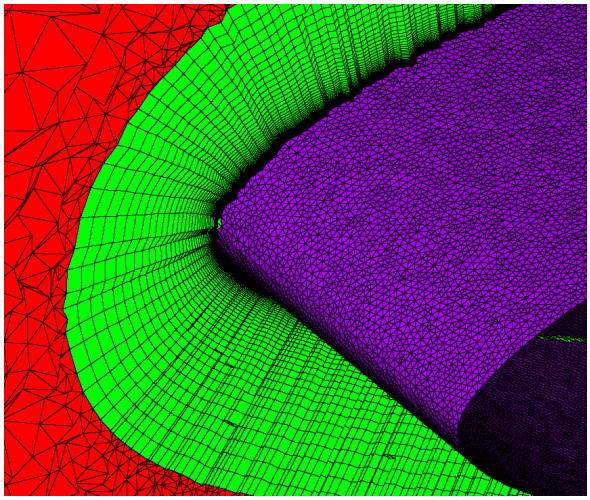

Figure 1: Hybrid ice accretion mesh.

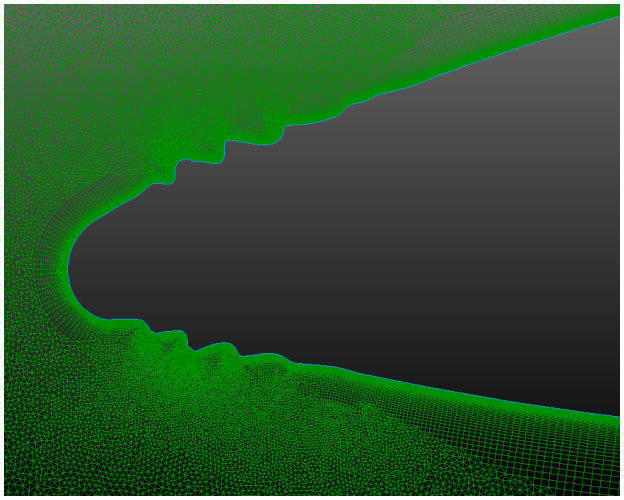

Figure 2: Performance calculation mesh with T-Rex.

Icing simulations were carried out as FENSAP-ICE multi-shot runs with automatic Fluent remeshing (Ozcer *et al.*, 2019). Each ice accretion run was simulated with 10 shots, monodisperse droplet distribution, and a constant ice density of ρ_{ice}=917kg/m³. The first shot was set to a shorter duration in order to capture the initial roughness build-up on the airfoil. Table 1 shows the duration of the shots for each simulation case. The grids for performance calculations were generated in Pointwise because T-Rex grids are very well-suited for complex geometries and offer a good resolution of the iced geometries.

The base geometry in this study was the RG-15 airfoil, which is a widely used design for UAVs and model airplanes. The airfoil has been used for numerical and experimental studies on UAV icing before (Fajt, Hann and Lutz, 2019; Hann, 2019). To investigate the effect of the chord length on ice accretion and performance penalties, the simulations were carried out on four chord lengths c=[0.11, 0.23, 0.45, 0.90 m], each at a velocity of v=25m/s. In order to assess the influence of the airspeed, four velocities v=[12.5, 25.0, 50.0, 100.0 m/s] were simulated on a chord of c=0.45m. Table 1 gives an overview of all the cases.

Three meteorological icing conditions were investigated for each of the flight configurations in Table 2. The basis for choosing meteorological icing conditions is the continuous maximum icing envelope in CFR 14, Part 25, Appendix C (Federal Aviation Administration, 2002). Icing conditions are chosen to represent the three main icing morphologies: rime, mixed, and glaze ice (Lynch and Khodadoust, 2001), and are shown in Table 2. Icing durations are calculated based on a horizontal extent of the stratiform icing cloud of 17.4nmi/32.2km (Federal Aviation Administration, 2002). The performance calculations of lift and drag were all conducted at the same Reynolds number Re=1×10^6 for easier comparison of the results.

Table 1: Flight conditions for the variation of chord length and airspeed and icing durations.

Velocity [m/s]	Chord [m]	Reynolds number	Icing duration [min]	1st shot duration [s]	2nd–10th shot duration [s]
12.5	0.45	0.5×10^6	43.0	60.0	280.0
25.0	0.45	0.9×10^6	21.5	30.0	140.0
50.0	0.45	1.8×10^6	10.8	15.0	70.0
100.0	0.45	3.6×10^6	5.4	7.5	35.0
25.0	0.11	0.2×10^6	21.5	30.0	140.0
25.0	0.23	0.5×10^6	21.5	30.0	140.0
25.0	0.90	1.8×10^6	21.5	30.0	140.0

Table 2: Overview of the meteorological icing conditions.

Variable	Glaze	Mixed	Rime
Temperature	−2 °C	−4 °C	−15 °C
MVD	20 µm	20 µm	20 µm
LWC	0.59 g/m³	0.55 g/m³	0.32 g/m³
AOA	0°	0°	0°

3. Validation

The accuracy and validity of simulation results is a key challenge for all studies that are based on numerical methods. Substantial validation work has been performed in previous work at NTNU. In particular, work has been conducted on investigating the grid dependency, the number of required shots for ice accretion, and the capability of FENSAP-ICE to predict aerodynamic penalties (Fajt, 2019; Hann, 2019; Hann *et al.*, 2020). This study followed the findings and experiences from these results and added a comparison of ice accretion simulations with FENSAP-ICE. For this, experimental ice shapes were obtained during icing wind tunnel tests at the Technical Research Centre of Finland (VTT) during fall 2019 (Tiihonen *et al.*, 2016). Two icing conditions were chosen to represent different ice accretion regimes. For each case, manual ice tracings were taken from each icing run at three different spanwise locations (Hann, 2019). The numerical simulations were conducted with the same CFD setup (mesh, turbulence model, mulit-shot) as stated in the method section. The results are shown in Figure 3. For mixed ice, the overall geometry of the ice seemed well-captured. However, the simulated ice shapes exhibited lower ice limits, lower ice thickness, and lower ice area. Ice area refers to the cross-sectional area of the ice accretion. The same differences also occurred for glaze ice, but in addition, there were horn features on the experimental ice shapes that were missing on the simulated ice accretion.

A detailed investigation of the potential reasons for the differences went beyond the scope and objective of this study. The most likely error sources included the assumption of constant ice density and a monodisperse droplet distribution for the simulations, as well as measurement uncertainties in the icing wind tunnel.

Although there were differences between the simulated and the experimental ice shapes, the differences were in line with the general capability of numerical icing codes, both on manned and unmanned aircraft (e.g. (Wright and Rutkowski, 1999; Szilder and McIlwain, 2011; Wang, Chang and Su, 2011)). Therefore, the validation results gave

confidence that the ice accretion physics were captured with sufficient accuracy to serve the purpose of this paper – which was to show general trends for variations of airspeed and chord length on ice accretion and icing performance.

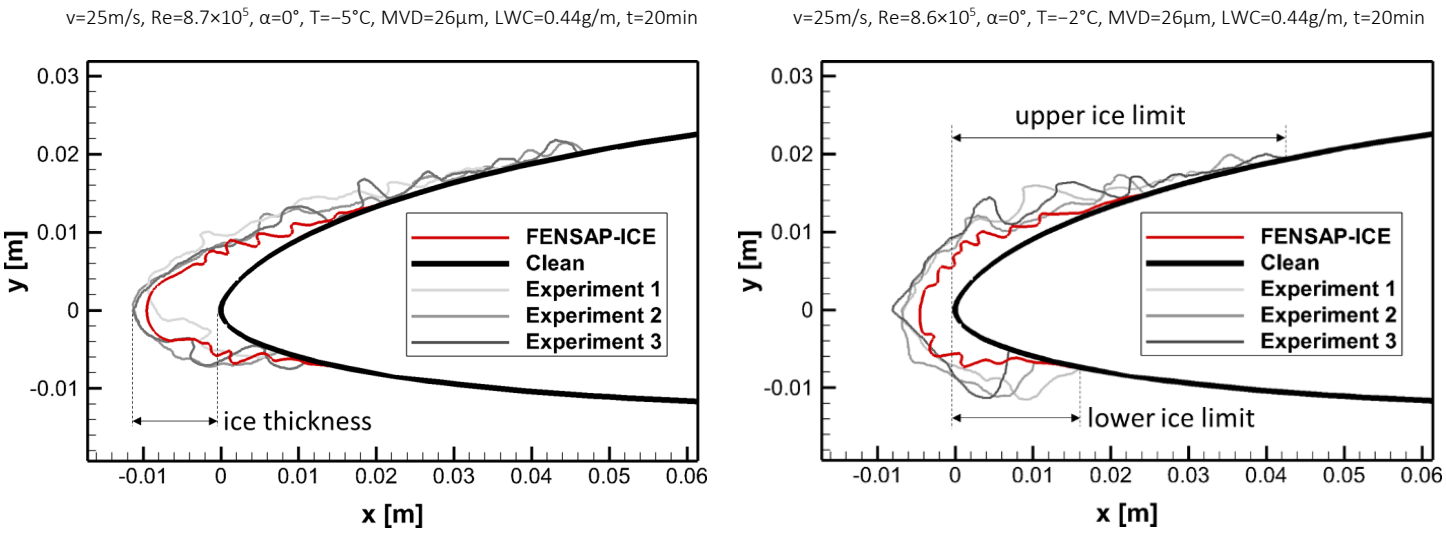

Figure 3: Comparison of FENSAP-ICE simulations with icing wind tunnel tests for ice accretions of mixed (left) and glaze (right).

4. Results

4.1 Ice Accretion

The resulting ice shapes for all the cases are shown in Figure 4. The airspeed had the lowest impact on the rime ice shapes (Figure 4, top, left). An increase in airspeed led to slightly increased relative ice thickness (i.e. maximum ice extent in relation to the chord length) and to a larger droplet impingement area. The ice geometry was a typical streamlined rime ice shape and the geometries were similar to each other at all airspeeds. The reason for these small differences was related to the low air temperatures – the ice accretion mechanism was governed by instant freezing of the incoming droplets. The increase in ice limits was directly related to the increase in impingement limits, which resulted from higher droplet inertias and thus higher collection efficiencies. This also led to an increase in relative ice thickness.

The airspeed had a larger impact on the mixed ice shapes (Figure 4, middle, left). The ice geometry at the lowest airspeed (red line) was almost identical in shape to the rime ice cases. This was related to the lower aerodynamic heating term, leading to a substantial increase in the freezing fraction. For higher airspeeds the aerodynamic heating increased, thereby decreasing the freezing fraction. Consequently, the mixed ice shapes became more convoluted and glaze-like. For v=25m/s the ice horn exhibited a distinct V-shape and large ice thickness. For higher airspeeds, the ice thickness decreased, and ice limits increased significantly. This was related to the higher aerodynamic heating, lower freezing fractions, and consequently higher runback water amounts. This led to higher ice limits and a reduction in ice thickness. For all airspeeds, except the lowest, the mixed ice shapes developed distinct horn structures. The size of these increased with higher airspeeds.

The airspeed had a significant influence on the glaze ice cases (Figure 4, bottom, left). At the lowest velocity, relatively high levels of instantaneous freezing occurred, which resulted in a streamlined ice shape. The similarity to rime was less compared to the low-speed mixed ice case. At higher velocities, the freezing fraction decreased substantially due to an increase in aerodynamic heating. This resulted in more complex ice shapes and significantly increased icing limits. For the highest velocity, the aerodynamic heating became so dominant, that the surface temperatures rose above the freezing point and no icing occurred on the airfoil. Instead, the surface was covered with a water layer over its entire length.

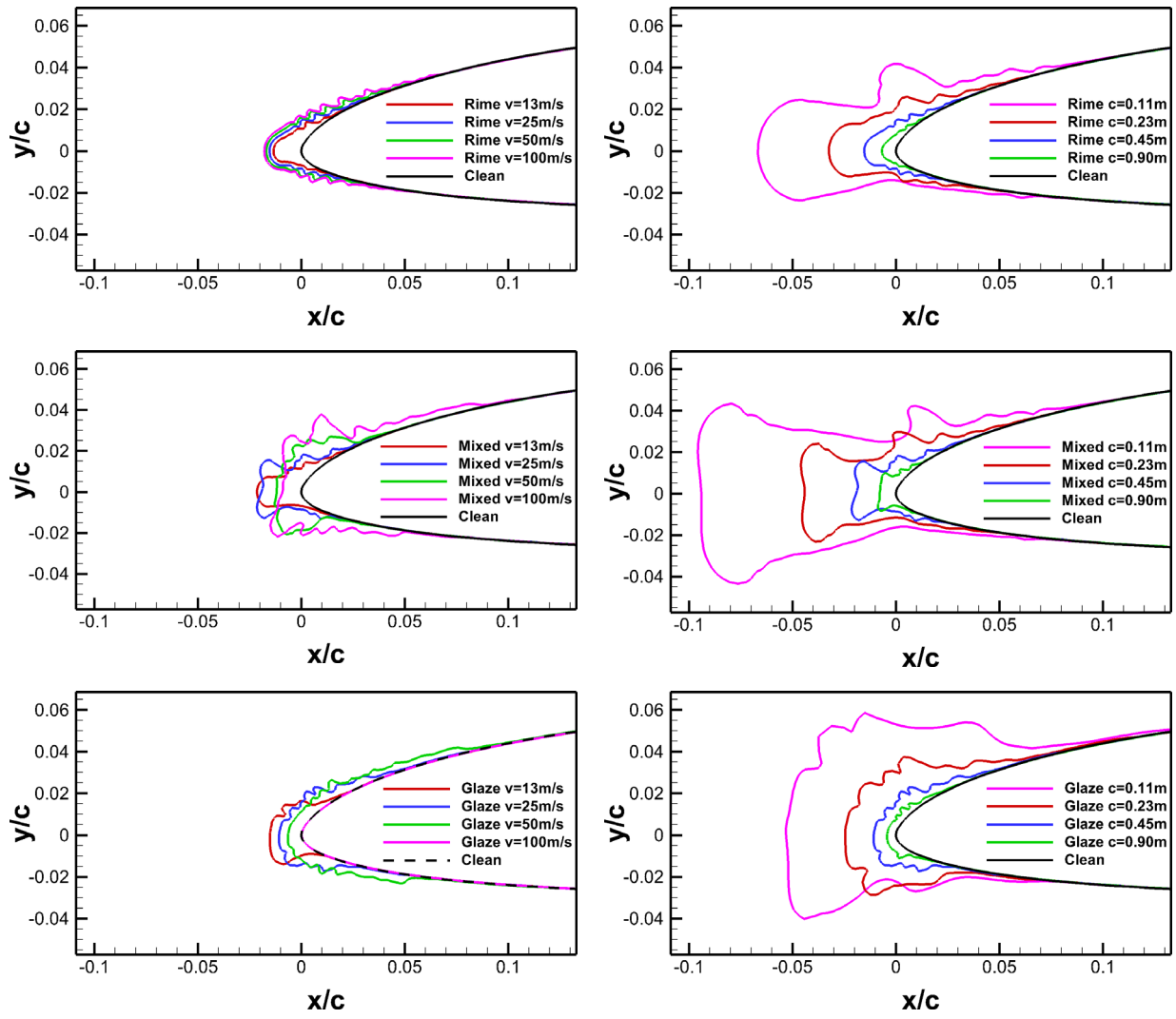

Figure 4: Ice shapes for the three meteorological icing conditions rime (top), mixed (middle), and glaze (bottom) for the variation of airspeed (left) and chord length (right).

The absolute ice mass for each simulation case is shown in Figure 5. For the airspeed variation, it shows that an increase in airspeed led to higher total ice accumulation. This was related to the higher droplet inertias and higher collection efficiencies. When aerodynamic heating exceeded a threshold value, the heating became so high that no ice formation would be possible. This only occurred for the glaze ice at the highest velocity. The reason why the rime ice masses are lower compared to the other cases, is related to the substantially lower LWC at lower temperatures, see Table 2.

The influence of the chord length of the airfoil was much more consistent between the three meteorological cases in Figure 4. The following effects were observed in all cases consistently. First, the relative ice thickness increased significantly for the smaller airfoils. Second, the relative ice limits increased significantly as well. Third, the ice shape geometry was not significantly affected by changes in chord length. This indicated that the ice accretion regime was not affected by the chord length.

This qualitative assessment was confirmed in Figure 5, showing that the absolute mass of ice was decreasing with smaller chord lengths. This means that while the relative ice thicknesses and the relative ice coverages on the smaller airfoils increased, the absolute ice masses decreased. Due to the lower size of the airfoil, the aerodynamic deflection forces are reduced, which results in a higher droplet collision efficiency. Thus, the relative ice thickness, droplet impingement area, and ice limits increased. Since the surface area for droplet impingement was smaller (due to the smaller airfoil geometry) a lower absolute number of droplets collide with the airfoil. This resulted in the lower absolute ice masses.

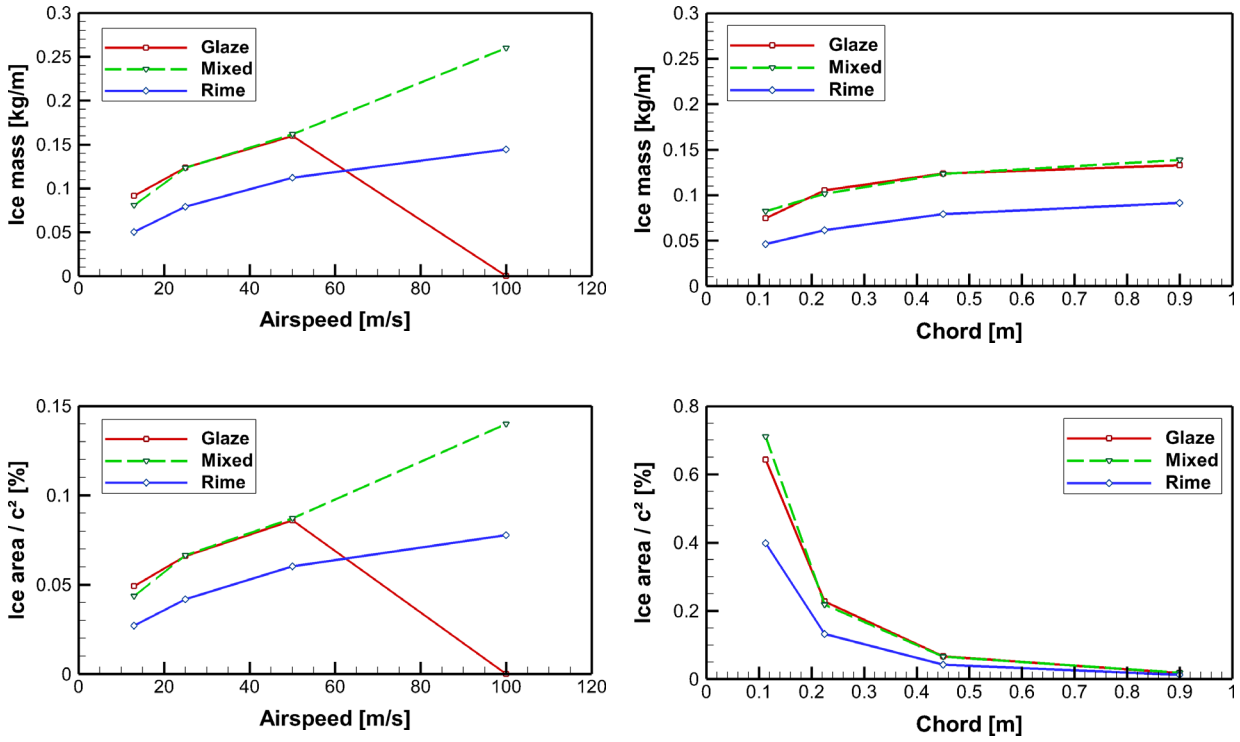

Figure 5: Total ice mass (top) and relative ice area (i.e. with regards to the chord *c* (bottom) for the variation of airspeed (left) and chord length (right).

4.2 Performance Penalties

First, the comparison was made between the clean airfoil with free transition and the three basic icing cases (rime, mixed, and glaze), see Figure 6. The results clearly showed the negative impact of the ice accretions. The stall angles were reduced by 2° from clean to iced cases. The maximum lift was reduced by $\Delta c_{l,stall}=(c_{l,stall,clean}-c_{l,stall,iced})/c_{l,stall,clean}$ = −12…30%, zero angle lift decreased by $\Delta c_{l,\alpha=0°}$= −5…8%, and zero angle drag increased by $\Delta c_{d,\alpha=0°}$= +110…170% depending on the ice type. Mixed ice showed the highest penalties and rime the lowest. A large part of this drag increase was related to the absence of laminar flow on the iced airfoils.

The impact of airspeed and chord length variation is shown in Figure 7. The airspeed variation on the rime ice geometries showed two separate effects (Figure 7, top, left). In the linear area (α< 7°) an increase in airspeed led to higher performance penalties, i.e. lower lift and higher drag. This was related to the increase in ice area and ice thickness. Consequently, the rough and uneven ice surface increased turbulence, leading to higher drag and lower lift. In the stall region, higher airspeeds led to a delay of stall and higher maximum lift values. This was related to the relatively streamlined form of the ice shape. The larger ice thicknesses acted extended the effect chord length and acted the same way as a leading-edge slat (high-lift device). This effect was only possible because the rime ice shapes were relatively streamlined and did not trigger larger flow separation areas.

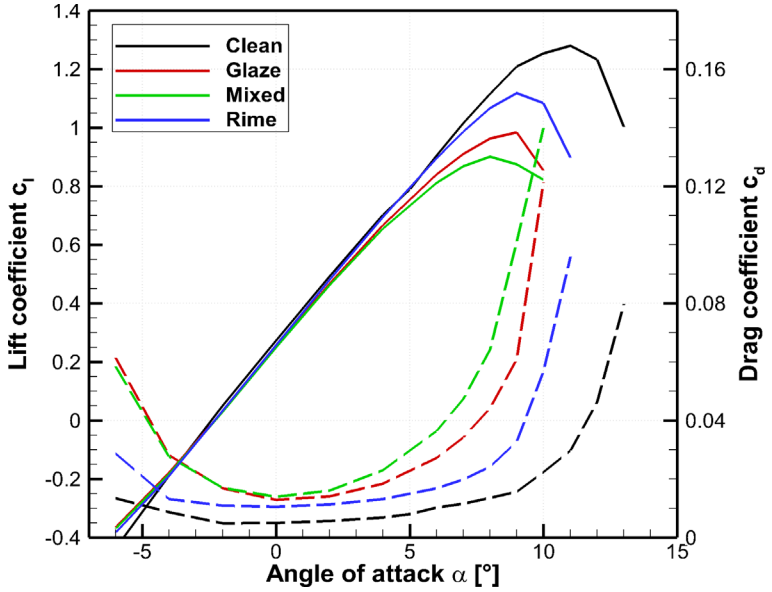

Figure 6: Comparison of the clean case with the three meteorological conditions rime, glaze, and mixed at airspeed *v*=25m/s and chord *c*=0.45m. Solid lines represent lift and dashed lines drag.

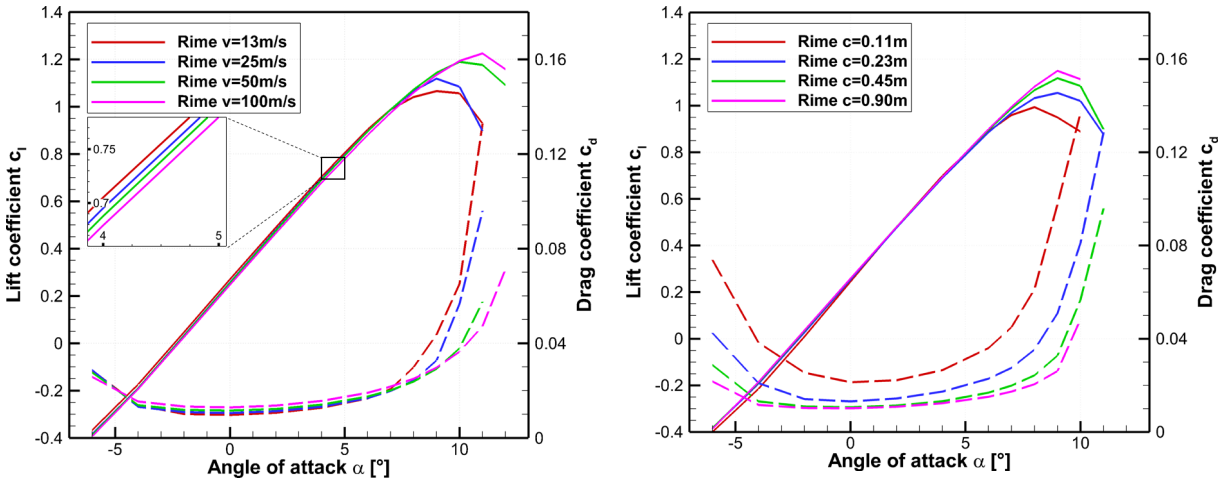

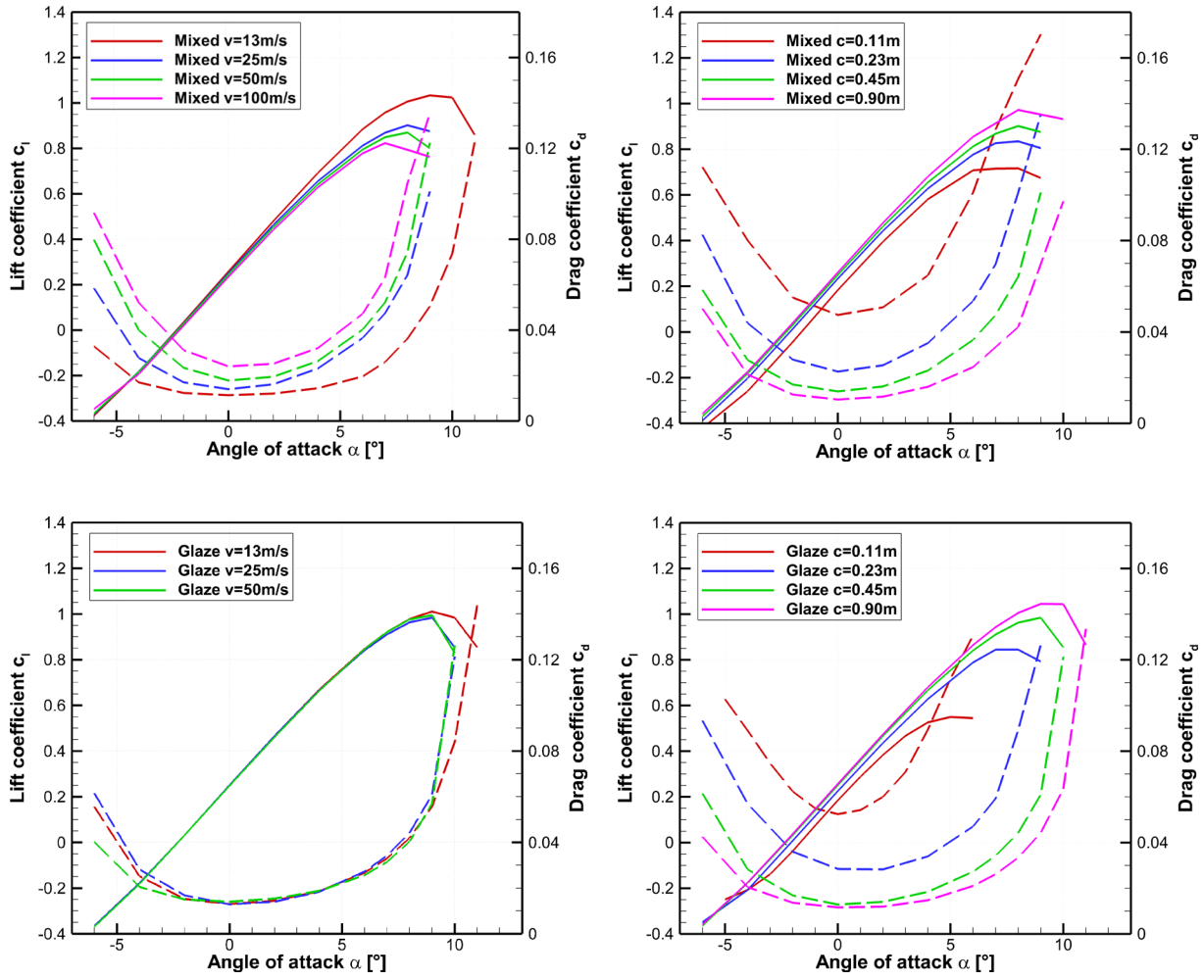

Figure 7: Aerodynamic performance for the three meteorological icing conditions rime (top), mixed (middle), and glaze (bottom) for the variation of airspeed (left) and chord length (right). Solid lines represent lift and dashed lines drag.

For mixed ice, the airspeed variation had a different effect (Figure 7, middle, left). The lowest performance penalties occurred for the lowest airspeed. In this case, that ice geometry was identical to a rime ice shape with streamlined from, resulting in low penalties. As airspeeds increased, the aerodynamic penalties increased as well. The ice shapes at the higher airspeeds all exhibited ice horns that led to large aerodynamic separations at the leading-edge, resulting in substantial performance losses. As the size of the ice horns increased at higher airspeeds, the aerodynamic performance degradation increased as well.

The variation of the airspeed resulted in a significant variation of the glaze ice geometries (Figure 7, bottom, left). These cases were dissimilar to each other with regards to ice mass, ice limits, and relative ice thickness. However, the performance penalties on the glaze ice shapes were very similar to each other. This can likely be explained by the inverse correlation between relative ice thickness and relative ice area. At low airspeeds the relative ice thickness was large, resulting in large separation zones. At higher airspeeds the ice thickness was smaller but the ice area was larger. No large ice horns built at larger airspeeds, in contrast to mixed ice. At high airspeeds, the size of the leading-edge

separations decreased, while due to the large surface coverage by ice, the roughness effects increased. This can be seen in Figure 8, where the ice shape at lower speeds results in a large separation area, whereas in the higher speed case the ice area is larger but results in weaker flow separation. These two effects seemed to be in balance with each other, which resulted in very similar performance penalties in all cases.

The effect of the chord length variation on the performance penalties of the rime ice shapes showed a clear trend in (Figure 7, top, right): A decrease in chord length led to larger relative ice thicknesses and larger relative ice area, which resulted in larger aerodynamic performance penalties.

For mixed ice, the same trends occurred (Figure 7, middle, right). For lower chord lengths, the relative ice thicknesses, ice area, and icing limits increased and led to higher degrees of aerodynamic penalties. The effect was non-linear, and substantially larger penalties occurred for the lowest airfoil size compared to the largest, especially on drag.

The glaze ice cases followed this trend as well (Figure 7, bottom, right). Lower chord lengths led to higher penalties. In particular, the largest overall penalties occurred for the glaze ice on the smallest airfoil. This was related to the large flow separations that occurred on the upper and lower side of the airfoil.

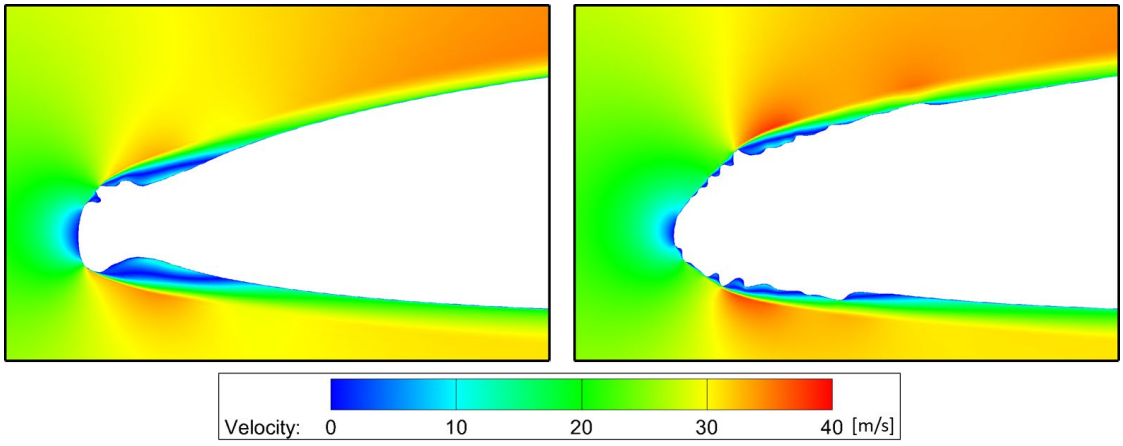

Figure 8: Flow separation on the leading-edge on the glaze ice shape at v=25m/s (left) and v=100m/s (right).

Discussion

The objective of this of study was to investigate the effect of airspeed and chord size on the ice accretion and aerodynamic performance of a UAV airfoil with numerical simulations. The results revealed several mechanisms. The variation of the airspeed showed two opposite effects, depending on the icing regime. In low-temperature cases (rime ice), an increase in velocity primarily resulted in higher droplet inertias and thus increased droplet collection efficiencies. Consequently, the ice shapes had larger relative ice thicknesses, larger ice areas, and larger ice mass. This led to higher aerodynamic penalties. At the same time, the larger rime ice horns acted as leading-edge slates which delayed stall to slightly higher angles of attack – but still below the values of the clean case.

At temperatures closer to the freezing point – where a substantial part of the incoming droplets would not freeze instantly (mixed & glaze ice) – an increase in airspeed led primarily to an increase in aerodynamic heating. As a result, the instant freezing fraction decreased, generating an increased amount of runback water. Generally, this led to lower ice thicknesses and higher ice limits. For the mixed ice cases, this shift resulted in the formation of very large ice horns and in substantial performance losses. For glaze ice, the ice shapes did not form horns and thus the performance losses did not increase significantly. For glaze, at the highest airspeed, the freezing fraction would decrease to zero as the surface temperature would rise to positive degree values. This prevented any ice formation.

The difference between the two aforementioned mechanisms was clearly showcased with the mixed ice cases. For the lowest airspeed, the ice type was streamlined rime with low performance penalties. For higher airspeeds, horn formation occurred due to the availability of runback water, which consequently led to high performance losses. This indicates that the transition zone between rime and glaze conditions may result in significant icing penalties and should be investigated further.

The variation of the chord length showed the same trend for all icing conditions. For smaller airfoil dimensions, the relative ice thicknesses and the specific ice area increased, whereas the absolute ice mass decreased. In all cases, the lower chord lengths generated larger aerodynamic penalties. However, there were differences in the degree of the changes. For rime ice, the increase in penalties was the smallest and for glaze ice the largest. This was most likely related to the more complex glaze ice shapes compared to the streamlined rime ice shapes.

These findings were in good agreement with the work of Szilder and McIlwan on the effect of the Reynolds number (with coupled airspeed and chord) on ice accretion physics (Szilder and McIlwain, 2011). Their finding, that the total ice mass decreases at lower Reynolds numbers, has been shown in this study to occur independently for airspeeds and chord length variations. Their finding that the relative ice area increases with lower Reynolds numbers was shown in this study to be primarily driven by the decrease in chord length. Decreasing airspeed also led to lower relative ice areas, but at a much lower rate compared to the effect of the decreasing chord lengths.

The understanding of these mechanisms is highly relevant as they showcase the differences between icing on UAVs and manned aircraft. Most UAVs are typically smaller and fly slower than large passenger aircraft (airliners) and even most aircraft found in general aviation. The results indicate that icing on UAVs can occur at temperatures at which insignificant icing would occur on manned aircraft. Also, changes in airspeed can lead to shifts in the ice accretion regime which can drastically change the ice shape geometries consequently leading to much higher penalties (e.g. going from rime to mixed).

This work also demonstrated that the smaller size of UAVs leads to larger relative ice thicknesses and larger performance penalties. This effectively means that UAVs are significantly more sensitive to icing conditions compared to

manned aircraft. Indirectly, this also means that low LWC conditions, which result in low ice accretion rates that may be less significant for manned aircraft, can be more severe for UAVs.

This does have a very important implication for icing nowcasting and forecasting methods. These numerical weather models typically predict an icing severity index that is calibrated for manned aircraft. Icing conditions which are evaluated as “trace” or “light” for manned aircraft (Jeck, 2001) may be severe for smaller UAVs. This highlights the need to develop suitable icing forecasting tools specifically for UAV applications.

The limitations of this study are mostly related to the quality of the numerical simulations of ice accretions and aerodynamic performance. Previous work and this validation have shown that FENSAP-ICE generally is able to capture the main icing features but is limited in predictive power when it comes to details. Hence, it is important to highlight that the simulated performance penalties in this study may differ from real icing conditions and that more validation work is needed. However, the general trends and mechanisms that have been revealed by this study are in line with previous work and are expected to be valid qualitatively, if not quantitatively.

Summary

Numerical simulations were carried out to investigate the effects of variation of airspeed and chord size on the aerodynamic icing penalties on a UAV airfoil. Three different meteorological icing conditions, based on the continuous maximum icing envelope for manned aircraft, were used to generate rime, mixed, and glaze icing regimes.

The results showed that the ice accretion regime had a significant influence on the resulting ice geometries, which were linked to the degree of aerodynamic performance penalties. The ice accretion regime was driven by temperature and airspeed (aerodynamic heating). For rime ice conditions an increase in velocity led to higher total ice mass and relative ice thicknesses, resulting in an increase in performance penalties. It was shown that the streamlined rime ice shapes can also delay stall. For glaze ice conditions an increase in velocity led to an increase in ice mass and area, but with thinner relative ice thicknesses and a larger coverage of the airfoil. The aerodynamic penalties did not change significantly with airspeed variations for glaze. At high velocities, the aerodynamic heating effect became so high that the surface temperatures on the airfoil rose above freezing and no ice accretion occurred. For mixed ice conditions, a shift from the rime-like behavior to the glaze-like behavior occurred for increasing velocities. The transition phase generated large ice horn features associated with very high aerodynamic performance degradation.

The variation of chord length had similar effects at all icing conditions. A decrease in chord length led to a decrease in total ice mass but an increase in relative ice area, relative ice thickness, and extended icing limits. This led in all cases to substantially higher aerodynamic performance penalties.

UAVs are smaller in size than manned aircraft and operate at lower flight velocities. This study showed that both these characteristics likely lead to UAVs being more sensitive to icing than larger manned aircraft. The lack of aerodynamic heating makes UAVs more susceptible to icing at near-freezing-point temperatures where icing would not occur on faster manned aircraft. The lower chord lengths led to larger ice horns relative to the airfoil size, which was connected to substantial performance penalties. The worst icing penalties occurred for small chord lengths and temperatures close to freezing – which may be commonly encountered by UAVs. This underlines the continued need for further research of icing effects on UAVs, especially at low Reynolds numbers.

Acknowledgments

This work has received funding from the Research Council of Norway under grant numbers 237906 Centre for Integrated Remote Sensing and Forecasting for Arctic Operations (CIRFA) and 223254 Centre for Autonomous Marine Operations and Systems (NTNU-AMOS). Further funding was received from the Norwegian Research Council FORNY, grant number 284649, and from the Regionalt Forskningsfond Midt-Norge, grant number 285248. The numerical simulations were performed on resources provided by the National Infrastructure for High Performance Computing and Data Storage in Norway (UNINETT Sigma2) on the Vilje supercomputer, under project code NN9613K Notur/NorStore.

References

ANSYS (2017) ‘ANSYS FENSAP-ICE User Manual 18.2’. ANSYS.

Bragg, M. B., Broeren, A. P. and Blumenthal, L. A. (2005) ‘Iced-airfoil aerodynamics’, Progress in Aerospace Sciences, 41(5), pp. 323–362. doi: 10.1016/j.paerosci.2005.07.001.

Chung, J. J. and Addy, H. E. J. (2000) A Numerical Evaluation of Icing Effects on a Natural Laminar Flow Airfoil. NASA Technical Report NASA/TM-2000-209775. doi: 10.2514/6.2000-96.

Fajt, N. (2019) The Influence of Meteorological Conditions on the Icing Performance Penalties on a UAV Airfoil. University of Stuttgart MSc Thesis.

Fajt, N., Hann, R. and Lutz, T. (2019) ‘The Influence of Meteorological Conditions on the Icing Performance Penalties on a UAV Airfoil’, in 8th European Conference for Aeronautics and Space Sciences (EUCASS). Madrid. doi: 10.13009/EUCASS2019-240.

Federal Aviation Administration (2002) 14 CFR Parts 25 and 29, Appendix C, Icing Design Envelopes. DOT/FAA/AR-00/30.

Gent, R. W., Dart, N. P. and Cansdale, J. T. (2000) ‘Aircraft icing’, Philosophical Transactions of the Royal Society of London. Series A: Mathematical, Physical and Engineering Sciences. Edited by G. Poots, 358(1776), pp. 2873–2911. doi: 10.1098/rsta.2000.0689.

Habashi, W. G. et al. (2004) ‘FENSAP-ICE : A Fully-3D in-Flight Icing Simulation System for Aircraft, Rotorcraft and UAVs’, in 24th International Congress of the Aeronautical Sciences. ICAS. Available at: http://www.icas.org/ICAS_ARCHIVE/ICAS2004/PAPERS/608.PDF.

Hann, R. (2018) ‘UAV Icing: Comparison of LEWICE and FENSAP-ICE for Ice Accretion and Performance Degradation’, in Atmospheric and Space Environments Conference. Atlanta: AIAA 2018-2861. doi: 10.2514/6.2018-2861.

Hann, R. et al. (2019) ‘Experimental Investigations of an Icing Protection System for UAVs’, in SAE Technical Papers. SAE Technical Paper 2019-01-2038. doi: 10.4271/2019-01-2038.

Hann, R. (2019) ‘UAV Icing: Ice Accretion Experiments and Validation’, in SAE Technical Papers. SAE Technical Paper 2019-01-2037. doi: 10.4271/2019-01-2037.

Hann, R. et al. (2020) ‘Experimental and Numerical Icing Penalties of an S826 Airfoil at Low Reynolds Numbers’, Aerospace, 7(46). doi: doi.org/10.3390/aerospace7040046.

Hann, R. and Johansen, T. (2020) Unsettled Topics in UAV Icing. SAE Edge Research Report.

Jeck, R. K. (2001) A History and Interpretation of Aircraft Icing Intensity Definitions and FAA Rules for Operating in Icing Conditions. Federal Aviation Administration Technical Report DOT/FAA/AR-01/91.

Lynch, F. T. and Khodadoust, A. (2001) ‘Effects of ice accretions on aircraft aerodynamics’, Progress in Aerospace Sciences, 37(8), pp. 669–767. doi: 10.1016/S0376-0421(01)00018-5.

Narum, E. F. L., Hann, R. and Johansen, T. A. (2020) ‘Optimal Mission Planning for Fixed-Wing UAVs with Electro-Thermal Icing Protection and Hybrid-Electric Power Systems’, in International Conference on Unmanned Aircraft Systems (ICUAS).

Ozcer, I. et al. (2019) ‘Multi-Shot Icing Simulations with Automatic Re-Meshing’, in International Conference on Icing of Aircraft, Engines, and Structures. SAE Technical Paper 2019-01-1956. doi: 10.4271/2019-01-1956.

Siquig, A. (1990) Impact of Icing on Unmanned Aerial Vehicle (UAV) Operations. Naval Environmental Prediction Research Facility Report.

Spalart, P. and Allmaras, S. (1992) ‘A one-equation turbulence model for aerodynamic flows’, in 30th Aerospace Sciences Meeting and Exhibit. doi: 10.2514/6.1992-439.

Steinbrenner, J. P. (2015) ‘Construction of prism and hex layers from anisotropic tetrahedra’, 22nd AIAA Computational Fluid Dynamics Conference, (June). doi: 10.2514/6.2015-2296.

Szilder, K. and McIlwain, S. (2011) In-Flight Icing of UAVs - The Influence of Reynolds Number on the Ice Accretion Process. SAE Technical Paper 2011-01-2572. doi: 10.4271/2011-01-2572.

Szilder, K. and Yuan, W. (2017) ‘In-flight icing on unmanned aerial vehicle and its aerodynamic penalties’, Progress in Flight Physics, 9, pp. 173–188. doi: 10.1051/eucass/201709173.

Tiihonen, M. et al. (2016) ‘VTT Icing Wind Tunnel 2.0’, in Winterwind Conference.

Tran, P. et al. (2004) ‘FENSAP-ICE Applications to Unmanned Aerial Vehicles (UAV)’, in 42nd AIAA Aerospace Sciences Meeting and Exhibit. Reno: American Institute of Aeronautics and Astronautics. doi: 10.2514/6.2004-402.

Wang, C., Chang, S. and Su, X. (2011) ‘Simulation of Ice Accretion on Three Dimensional Wing’, in. SAE Technical Paper 2011-38-0043. doi: 10.4271/2011-38-0043.

Williams, N. et al. (2017) ‘The effect of icing on small unmanned aircraft low Reynolds number airfoils’, in 17th Australian International Aerospace Congress (AIAC). Melbourne.

Wright, W. and Rutkowski, A. (1999) Validation Results for LEWICE 2.0. NASA Technical Report NASA/CR—1999-208690. doi: 10.2514/6.2005-1243.